PERFORMANCE ANALYSIS OF A NEW ULTRASOUND AXIAL STRAIN TIME CONSTANT ESTIMATION

A Thesis

by

SANJAY PADMANABHAN NAIR

Submitted to the Office of Graduate Studies of
Texas A&M University
in partial fulfillment of the requirements for the degree of

MASTER OF SCIENCE

May 2010

Major Subject: Electrical Engineering

Performance Analysis of a New Ultrasound Axial Strain Time Constant Estimation

PERFORMANCE ANALYSIS OF A NEW ULTRASOUND AXIAL STRAIN TIME CONSTANT ESTIMATION

A Thesis

by

SANJAY PADMANABHAN NAIR

Submitted to the Office of Graduate Studies of
Texas A&M University
in partial fulfillment of the requirements for the degree of

MASTER OF SCIENCE

Approved by:

Chair of Committee,	Raffaella Righetti
Committee Members,	Steven Wright
	Takis Zourntos
	Steven Riechman
Head of Department,	Costas Georghiades

May 2010

Major Subject: Electrical Engineering

ABSTRACT

Performance Analysis of a New Ultrasound Axial Strain Time Constant Estimation

(May 2010)

Sanjay Padmanabhan Nair, B.S., Texas A&M University

Chair of Advisory Committee: Dr. Raffaella Righetti

New elastographic techniques such as poroelastography and viscoelasticity imaging aim at imaging the temporal mechanical behavior of tissues. These techniques usually involve the use of curve fitting methods as applied to noisy data to estimate new elastographic parameters. As of today, however, image quality performance of these new elastographic imaging techniques is still largely unknown due to a paucity of data and the lack of systematic studies that analyze performance limitations of estimators suitable for these novel applications. Furthermore, current elastographic implementations of poroelasticity and viscoelasticity imaging methods are in general too slow and not optimized for clinical applications.

In this paper, we propose a new elastographic time constant (TC) estimator, which is based on the use of the Least Square Error (LSE) curve-fitting method and the Levenberg-Marquardt (LM) optimization rule as applied to noisy elastographic data obtained from a tissue under creep compression. The estimator's performance is analyzed using simulations and quantified in terms of accuracy, precision, sensitivity,

signal-to-noise ratio (SNR) and speed. Experiments are performed as a proof of principle of the technical applicability of the new estimator on real experimental data.

The results of this study demonstrate that the new elastographic estimator described in this thesis can produce highly accurate, sensitive and precise time constant estimates in real-time and at high SNR. In the future, the use of this estimator could allow real-time imaging of the temporal behavior of complex tissues and provide advances in lymphedema and cancer imaging.

ACKNOWLEDGEMENTS

I imagine when people read acknowledgements or dedicatory notes people expect to see a series of statements in which the author expresses gratitude they have that the people around them are who they are. It might be the way I was brought up or it might be the rebellious nature in me, but that's not my style. I think, in a way, expressing gratitude trivializes what these people mean to me. I say "thank you," to complete strangers who have just passed me the mustard that I'm about to lather on a hot dog and I say it without much feeling. Instead of writing an extremely corny letter of appreciation, I'm writing an even cornier and cheesier letter of joy, because that is the exact sentiment I have towards anybody mentioned here.

I still hold on to a very old-fashioned view of "University": a forum for people to come and discuss their opinions. There's a vision, that maybe together, as peers, and without prejudice, we can come up with a solution for the disease and madness that often bring misery to this world. I feel that my professor, Dr. Righetti, also has this vision in her mind. Even though it's considered unwise to complete all my post high school education in the same university, I'm looking forward to continuing my work with her and the TAMU Ultrasound Group. I don't often hear about professors so caring or patient with their students. Admittedly, this is a patience that I've oftentimes tested.

As for the rest of the ultrasound group, we're a small bunch but I also believe we're amongst the most close-knit groups in the ECEN department. It's true, Biren and I used to frequently butt heads, but now we get along excellently. I'd also frequently go over to Sthiti's to steal some of her tea and dinner, a fact which she uses as a counter-

argument against my claim that she's stingy. Anuj and I are pretty close friends to the point where it seems we can complete each other's thoughts and sentences. As for Xu Yang, I guess he seemed to me as the most shy but he knows how to take a good joke and is also quite fond of laughing. And finally, there's Raghu who would always sit facing the counter at the place we'd all go get coffee because he had a crush on one of the girls working the cash register.

As with my luck in finding such an amazing group to work with, I've been quite lucky to always have really cool people around me both inside and outside of the lab. I've had friends like Magdalena, Sicilia, Garret, Jessica, Amanda, Tiffany, Rodrigo, Chad, Justin, Grant, Hillary, and Tabitha, all of whom for some reason I always found I could easily talk to. These people are my knights and I hope I have the consistency of character to be theirs. If it's true that strangers judge a person by first judging who they keep around them, then I imagine people should think quite highly of me.

As a young child I was raised to believe that no matter how knowledgeable or wise I may become – a statement which should not be taken as a claim that I have achieved being either – I should never see myself as a superior to any of the people who have taught me throughout my developing years. It's true; whatever good is in me is instilled in huge part by them. I don't feel they come much cooler than the ones that have taught me throughout my childhood years. Two of the most influential with respect to how I carry myself are Renato and Frances. Frances, my eleventh grade English teacher, amazes me in that even though she has gone through some really hard and distressing times she has never complained about her fate and maintains a lionhearted

love for life which I find admirable. Renato, my twelfth grade math teacher, I haven't kept as much contact with as I do with Frances, but I enjoyed his style of teaching and his slightly rebellious but humble and approachable nature. I should note that I am addressing them by their first names because of my fondness for them, not because of some form of irreverence.

Every now and then, when I'm at home I sit in front of the television channel surfing. Sometimes, a documentary pops up showing an adorable image of an infant elephant doing something mischievous and foolish, but it looks like it's tremendous amounts of fun. He's usually running around recklessly or even just lying down there lazily. Eventually, an older elephant will come and make it so that whatever foolishness that creature is doing comes to a halt. This is the story that summarizes my existence: I am that little elephant. Gautham, my mother, and my father, have always been that older, care-taking figure.

TABLE OF CONTENTS

CHAPTER Page

LIST OF FIGURES

CHAPTER I

INTRODUCTION AND BASIC CONCEPTS

A. Introduction

This chapter defines the objectives of this study, the hypothesis to be proven, and also discusses the break-down of the problem into several smaller aims. Essential mechanics and signal processing concepts are also discussed in this chapter.

B. Objective and hypothesis

The main objective of this study is to analyze the reliability and feasibility of axial strain time constant imaging estimators. The hypothesis of this study is that axial strain time constant estimation can be done accurately and speedily using curve-fitting techniques.

C. Problem breakdown

Three issues are addressed in this work:

1. Design of a suitable time constant estimation algorithm
2. Design of a simulation procedure to evaluate the performance of the algorithm

---

This thesis follows the style of Ultrasound in Medicine and Biology.

3. Design of suitable experiments to corroborate simulation results

D. Relevant mechanics concepts

i. Strain

All solid bodies experience a deformation or displacement when a force is exerted upon them. We define the strain across an axis as:

$$S = \frac{L - l}{L} \qquad (1.1)$$

where S denotes strain and L and l denote the lengths across an axis before and after it is compressed respectively. It is worth noting that the strain S as defined above is a unitless quantity and can be viewed as a fraction or percentage. Furthermore, the definition of strain S under this equation suggests that a compression implies a positive strain and an elongation or stretching implies a negative strain. This is, in fact, the opposite of the definition of a strain used in several texts, but is a frequently used one in the elastography community.

ii. Tissue's time constant

This study emphasizes the study of the temporal mechanical properties of a tissue. When placed under a constant compressive force (i.e. a creep test), a poroelastic material experiences a time dependent strain which reaches an equilibrium value after a

period of time. This behavior is modeled by the following equation (Qiu et al. 2008, Sridhar et al. 2007, Righetti et al. 2005):

$$S(t) = \eta + (\propto -\eta)e^{\frac{-t}{\tau}} \qquad (1.2)$$

where $S(t)$ denotes the strain at time t, η denotes the equilibrium strain value reached when $t = \infty$, α denotes the strain at time $t = 0$, and τ denotes the axial strain time constant. Informally speaking, τ can be interpretted as a measure of how quickly the material reaches its equilibrium value η. Note that both τ and η are in general unknown and need to be estimated.

iii. Practically viable assumptions

Equation 1.2, describing the temporal behavior of a tissue under a compressive force, shows that the equilibrium strain value is reached, strictly, only at time $t = \infty$. This would imply that to fully capture all the data pertaining to a creep curve for a tissue, one would have to record strain values for an indefinitely long period of time. This is, without a doubt, an impossible feat to achieve.

Recollection of circuit theory shows that this creep curve behaves similarly to the transient response of a resistor-inductor (RL) circuit. An RL circuit reaches an equilibrium, strictly at time $t = \infty$ but at a rate that can be interpreted in terms of its time constant τ. An approximation frequently used in the circuit theory community is that the transient response of an RC circuit reaches equilibrium at 5 times the value of its time constant (Nilsson and Riedel, 2005). This implies that after a "long enough" period of

time all increases seen in the transient response can be considered to be negligible. Likewise, for the creep curve of a poroelastic tissue it should be possible to make an equivalent approximation. This approximation becomes a matter of significant relevance that is treated in the portions of this study pertaining to the methods with which axial strain time constants are estimated from experimental data.

E. Relevant signal processing concepts

i. Sampling

This creep curve can be seen as a signal. As with all experimental data acquisition involving a digital system, it is impossible to acquire this signal for all real t as an analog signal. The best that can be done is to acquire $S(t)$ in terms of a series of samples $S(t_i)$ such that:

$$S(t_i) = \eta + (\propto -\eta)e^{\frac{-t_i}{\tau}} \qquad (1.3)$$

Fortunately, as shown by the Nyquist-Shannon sampling theorem, it is possible to completely reconstruct a signal if the sampling frequency is greater than twice the signal's maximum frequency, then the signal is fully reconstructible from its samples using Fourier reconstruction (Shannon 1949). In a strict sense, the study concerning this thesis does not make heavy use of the Nyquist-Shannon sampling theorem and Fourier reconstruction. However, it is used in several occasions in this thesis to explain the effect that sampling has on the performance of several of the algorithms explored in this study.

ii. Noise

The equation for $S(t_i)$ shows an unrealistically optimistic expression of what is truly acquirable by an experimental setup. In reality, all samples $S(t_i)$ are affected by noise $N_i(t_i)$. Each sample is more accurately expressed by:

$$S^{\dagger}(t_i) = \eta + (\propto -\eta)e^{\frac{-t_i}{\tau}} + N_i(t_i) \qquad (1.4)$$

where $N_i(t_i)$ is a random variable which is assumed to have a 0-mean Gaussian distribution. The noise distributions assumed in all simulations in this study follow a constant SNR among the strains, implying a variable standard deviation across all $N_i(t_i)$. The signal to noise ratio (SNR), in dB, for a stationary signal can be measured as:

$$SNR(dB) = 20log_{10}(\frac{\mu_{signal}}{\sigma_{signal}}) \qquad (1.5)$$

For a particular noisy strain $S^{\dagger}(t_i)$, $\mu_{signal} = S(t_i)$ as $N_i(t_i)$ is zero-mean. Furthermore, $\sigma_{signal} = \sigma(N_i(t_i))$, since $N_i(t_i)$ is the only source of variation for the signal. Therefore, for a particular SNR, the expression for $\sigma(N_i(t_i))$ becomes:

$$\sigma\big(N_i(t_i)\big) = \frac{S(t_i)}{10^{\frac{SNR(dB)}{20}}} \qquad (1.6)$$

As discussed in chapter VI, the calculation of strains is done by an additive method. This additive method forces the condition that $\sigma(N_{i+1}(t_{i+1})) > \sigma(N_i(t_i))$. Below, we provide a proof of this condition:

Let $N(t,u)$ denote the noise for the strain estimate $S(t,u)$. Thus:

$$S^{\dagger}(t_i) = S^{\dagger}(t_{i-1}) + S^{\dagger}(t_{i-1}, t_i)$$

$$S^{\dagger}(t_i) = S(t_{i-1}) + S(t_{i-1}, t_i) + N(t_{i-1}) + N(t_{i-1}, t_i)$$

$$S^{\dagger}(t_1) = S(t_0, t_1) + N(t_0, t_1)$$

From this it is easy to see that:

$$N(t_i) = N(t_{i-1}) + N(t_{i-1}, t_i) = \sum_{k=1}^{i} N(t_{k-1}, t_k)$$

Assuming all $N(t_{k-1},t_k)$ to be 0 mean Gaussian distributed random variables that are independent of each other then it is possible to express each $N(t_{k-1},t_k)$ as a product of a Normally distributed random variable X with a mean of 0 and a standard deviation of 1, and $\sigma(N(t_{k-1},t_k))$. Let $\sigma_{k-1,k} = \sigma(N(t_{k-1},t_k))$, then

$$N(t_i) = \sum_{k=1}^{i} \sigma_{k-1,k} X = \left(\sum_{k=1}^{i} \sigma_{k-1,k} \right) X$$

Since $\sigma_{k-1,k} > 0$ then it follows that $\sigma(N(t_i)) > \sigma(N(t_{i-1}))$. Furthermore, it is relevant to note that all $N(t_i)$ also have a zero-mean Gaussian distribution. Q.E.D.

This proof allows for some convenient simplification on the noise model of the strain vs. time plots. All strain vs. time plots are assumed to have a constant SNR along the strains. As shown in equation 1.6, a constant SNR along all $N_i(t_i)$ suggests that $\sigma(N_i(t_i))$ is increasing as i increases. This assumption also accounts for the fact that smaller increases in $S(t_i)$ correspond to smaller increases in $\sigma(N_i(t_i))$, a notion that is consistent with the nature of axial strain elastography. Therefore, it is correct to say that a constant SNR along the strains is a reasonable assumption.

The discussion on noise models is very relevant to this study. Noise becomes an integral part when discussing time constant estimation. All estimation done from

experimental data must be done in a form consistent with the noise model assumed for the data.

CHAPTER II

PRIOR ADVANCES IN ULTRASOUND AXIAL STRAIN TIME CONSTANT IMAGING

A. Introduction

I have very rarely heard of research that provides progress in a field that does not base itself on advances that have been provided by others. This chapter provides the background behind the work discussed in this thesis.

B. Ultrasonic elastography or strain imaging

Ultrasound elastography is a well-established imaging modality, which can be used for detecting a variety of pathological conditions in tissues (Garra et al. 1997, Hall et al. 2003, Itoh et al. 2006, Thomas et al. 2006, Svensson et al. 2006, Emilianov et al. 1995, D'hooge et al. 2002, Sandrin et al. 2003, Souchon et al. 2003). Standard elastography techniques generate what is usually referred to as an "axial strain elastogram", which is an image of the strain tensor component along the axis of insonication (i.e. the axis along which ultrasound radiation is being emitted). Axial strain elastograms have been shown to be highly correlated with changes in the corresponding

underlying tissue stiffness distribution (Srinivasan et al. 2004). Elastography has opened up a new field in ultrasound imaging, and is becoming an important clinical tool for the diagnosis of a number of pathological conditions.

C. Imaging the temporal mechanical behavior of tissues

With axial strain elastography as a tool for imaging a tissue's stiffness, several novel emerging elastographic techniques were proposed that may allow the imaging of additional mechanical properties of tissues related to their behavior under mechanical loads or stresses (Konofagou et al. 2001, Righetti et al. 2005). Amongst the latest advances in ultrasonic imaging were poroelastography and viscoelasticity imaging. Poroelastography is the application of elastography techniques for imaging the temporal behavior of materials that, because of their relatively high fluid content and mobility, can be modeled as poroelastic (Righetti et al. 2004, Berry et al. 2006). In a similar manner, viscoelasticity imaging methods apply elastography techniques to image the temporal behavior of materials that can be modeled as viscoelastic media (Sack et al. 2008, Liu and Ebbini 2008, Sridhar and Insana 2007). These elastographic techniques may be deployed using a number of experimental testing protocols, such as creep and stress relaxation tests (Konofagou et al. 2001, Ammann et al. 2006) or by applying low frequency vibrations to tissues (Krouskop et al. 1987).

Application of these techniques may allow generation of new types of elastograms that are related to the tissue poroelastic and viscoelastic behavior. These include: the effective Poisson's ratio (EPR) elastogram (EPR is the ratio of transverse strin vs. axial strain); the axial strain time constant (TC) elastogram, tackled in this work; the effective Poisson's ratio TC elastogram and the permeability elastogram (permeability measures the "ease" with which fluid flows in a poroelastic material) (Righetti et al. 2005, Righetti et al. 2007b). These new types of elastograms have the potential to convey new tissue information, which may prove clinically useful for the detection and staging of different tissue pathology, physiology and functional conditions. Medical areas where the application of these techniques could have a significant impact include cancer imaging and the detection and staging of lymphedema. While a number of studies have shown that elastic strain images of breast tissue can be effective at discriminating focal benign and malignant tumors (Thomas et al 2006, Thomas et al 2007, Zhi et al 2007, Itoh et al 2006), Qiu et al. (2008) found that the characterization of nonpalpable breast lesions is improved by the addition of viscoelastic strain imaging parameters. Imaging the temporal behavior of tumors may provide information about the stage of a cancer, which is known to be related to the tumors' fluid content and mobility. Similarly, preliminary poroelastographic experiments on lymphedema tissues *in vivo* have suggested that axial strain elastograms and effective Poisson's ratio elastograms and their temporal evolution under load may convey important diagnostic information to distinguish between normal and lymphedematous tissues (Righetti et al. 2007a, Berry et al. 2008).

Elastographic imaging of poroelastic and viscoelastic materials has been accomplished by generating time-sequenced axial strain elastograms or EPR elastograms while subjecting the material to a constant axial strain (stress relaxation) or a constant axial stress (creep). Given a set of temporal elastograms as obtained from a poroelastic or viscoelastic material, it is possible to generate TC elastograms, which depict the temporal behavior of the elastographic parameter of interest (for example the axial strain). TC elastograms are generated by applying curve fitting techniques to experimental elastographic data to estimate the TC of the elastographic parameter of interest on a pixel-by-pixel basis (Righetti et al. 2005, Righetti et al. 2007b). While the theoretical model used in these techniques depends on assumptions about the tissue behavior (i.e., poroelastic, viscoelastic, etc.), elastographic TC imaging usually involves the use of curve fitting methods as applied to *noisy* elastographic data. The accuracy of the resulting TC estimates is expected to depend on the curve fitting method employed, the length of the window of observation, the sampling period at which the elastographic data are acquired and the level of noise on the elastographic data (Bendat and Piersol 1986). A complication that arises in the application of curve-fitting methods for poroelastography is that, in practical cases, the models usually contain multiple unknown parameters due to the biphasic nature of the poroelastic tissues. Therefore, more than 1 parameter needs to be estimated from the same curve. To my knowledge, image quality performance of poroelasticity and viscoelasticity elastographic imaging is still largely unknown due to a paucity of data and the lack of systematic studies that analyze performance limitations of estimators suitable for these novel applications.

CHAPTER III

CURVE FITTING ARGUMENT SELECTION

A. Introduction

Elastographic time constant imaging can be summarized as a curve fitting problem, which itself usually involves comparing a theoretical noiseless test curve to the noisy experimental data and find the curve that best "fits" the data with respect to a goodness of fit measure. This chapter discusses the different goodness of fit arguments considered while developing tools for time constant estimation.

B. Maximum correlation

The first goodness of fit measure considered was correlation. In this scheme, the best theoretical fit is assumed to be the noiseless curve that is the most correlated to the data. This was chosen as a candidate method because maximum correlation used to be considered the argument of choice (Righetti et al. 2005, Righetti et al. 2007b). This method was quickly discarded for this study because the calculation of this argument is computationally demanding and therefore not suitable for clinical applications. This problem was exacerbated by the fact that the optimization methods devised at that time were themselves slow.

C. Least square error approaches

Least Squared Error curve-fitting is a popular family of methods for extracting parameters of a mathematical model from a given set of experimental data. In these curve-fitting schemes, the best fit is taken to be the one for which an error metric is seen to be the smallest. Thus, for a mathematical model corresponding to a function of time $f(t)$ with two parameters, τ and η, and for a set of n data points $S^{\dagger}(t_i)$, least square error curve fitting returns η and τ that minimizes:

$$LSE(f(t,\eta,\tau)) = \sum_{i=1}^{n} E(f(t,\eta,\tau), S^{\dagger}(t_i)) \qquad (3.1)$$

where E is an error metric function between $S^{\dagger}(t_i)$ and $f(t,\eta,\tau)$. Two Least Squared Errors approaches were considered in this study: General Least Squared Error (GLSE) curve-fitting and also Standard Least Squared Errors (SLSE) fitting.

D. General least squared error (graphical error minimization)

General least square error curve fitting involves minimization of the so-called geometric error:

$$E\left(f(t,\eta,\tau), S^{\dagger}(t_i)\right) = min_{\mathrm{t}}\left(\left(f(t) - S^{\dagger}(t_i)\right)^2 + (t - t_i)^2\right)$$

It is called the geometric error because it is the minimum Euclidean distance between the experimental data point and the plot of a given noiseless theoretical error. Notable in this

scheme is that times t and t_i must be first made unitless. Since, t and t_i are measured in units of time (e.g. seconds), the sum $(f(t)-S^{\dagger}(t_i))^2 + (t-t_i)^2$ cannot be computed "as is" because $f(t)$ and $S^{\dagger}(t_i)$ are unitless quantities.

E. Problems with GLSE

GLSE was implemented and tested yielding good results with respect to accuracy and precision. However, before further testing and optimization was done, several issues were discovered with this scheme. One issue was related to the scaling factor used to make t and t_i dimensionless. In this case, as t is measured in seconds, this is done by dividing the value of t by multiplying by 1/s. However, it should be perfectly acceptable to have t measured in milliseconds, instead of seconds, in which case normalization could be done by multiplying by 1/ms. This can be seen as a modification in the scaling of the strain vs. time plot. The problem is that doing this will, in general, change the results of the best fit, making the use of this form of GLSE return a curve with a different τ and η than what it would return with a different plot scaling.

The biggest issue with using this form of GLSE estimation is that it does not match the noise model assumed. To be accurate and consistent, the noise model has to be such that the time measurements t_i, as well as the strain measurements $S^{\dagger}(t_i)$) have to be affected by additive noise with distributions that are jointly Gaussian and also identically distributed. It is true that the measurements do in fact have some degree of uncertainty (noise) with respect to t_i measurements. However, the standard deviation of the noise of

t_i is so small when compared to that of $S^{\dagger}(t_i)$ that this variation can be ignored. Furthermore, since the calculation of the error metric for each data point t_i and $S^{\dagger}(t_i)$ involves the computation of a minimum, GLSE estimation can be a time taking process. For these reasons, the use of GLSE estimation was considered not suitable for our study and a standard least square error (SLSE) curve-fitting scheme was considered instead.

F. Standard least squared error (algebraic error minimization)

After the use of GLSE estimation was concluded to be inappropriate, it was found that SLSE was the more correct means of time constant estimations. SLSE involves the minimization of the so-called algebraic error:

$$E\left(f(t,\eta,\tau),S^{\dagger}(t_i)\right) = \left(f(t) - S^{\dagger}(t_i)\right)^2 \qquad (3.2)$$

SLSE avoids the issue of the need for the time, *t*, measurements to be unitless. As well, plot scaling has no effect on the resulting estimation. Finally, since SLSE is best suited for scenarios in which the noise model for the data samples acquired is Gaussian, the error metric is appropriate for this application.

G. SLSE shortcomings

SLSE returns a most likely fit when all the data samples are affected by additive noises that have independent and identically distributed Gaussian noise distributions. This implies that $\sigma(N_1(t_1)) = \sigma(N_2(t_2)) = \ldots = \sigma(N_n(t_n))$. However, it's already proven that

the correct relationship for the standard deviations of the noise distributions is $\sigma(N_1(t_1)) \leq \sigma(N_2(t_2)) \leq \ldots \leq \sigma(N_n(t_n))$. Furthermore, since $N_i(t_i) = N_{i-1}(t_{i-1}) + N(t_{i-1},t_i)$ the noise distributions are independent of each other. These complications are not ignored in this study. In truth, SLSE will return a fit that is an estimate of the most likely fit.

It is worth noting that probably the best LSE approach to be used for this kind of estimation would be a weighted SLSE approach, in which the error metric would be given a different weight:

$$E_i\left(f(t,\eta,\tau),S^{\dagger}(t_i)\right) = w_i\left(f(t) - S^{\dagger}(t_i)\right)^2$$

where each w_i would be inversely proportional to $\sigma(N_i(t_i))$. However, establishment of what value to assign w_i to requires accurate estimation of $\sigma(N_i(t_i))$ which is a challenging task beyond the scope of this study.

CHAPTER IV

CURVE FITTING OPTIMIZATION

A. Introduction

Curve-fitting usually involves a trial-and-error numerical process by which an argument function is either maximized or minimized. This process is a frequently tackled topic in the field of numerical analysis and optimization. This chapter discusses the different optimization methods tried in this study.

B. Linear search optimization

A linear search optimization technique was the first algorithm implemented in this study in unison with the maximum correlation curve-fitting argument. In this optimization scheme, the value of η is considered to be the last strain value acquired for the sampled strain vs. time plot.

Linear optimization finds the best fitting τ by: considering all candidate values of τ in a specified range, testing the goodness of fit with respect to an argument function, and then finding which one returns the best goodness of fit. This optimization technique was only used to process preliminary data results and was quickly substituted because of its exceedingly long runtime: on the order of days for a typical axial strain TC elastogram. Furthermore, since the value for η was not estimated, and simply assumed

from the last point of a given strain vs. time plot, the performance of the curve-fitting argument and optimization combination was data dependent, yielding lower accuracy and precision for time constant curves with higher τ values.

C. Bisection method optimization

The bisection method follows a similar optimization process as linear search in that it assumes the value of η to be the last value of the sampled strain vs. time plot. However, it is a much faster algorithm that follows a search process similar to binary search in that at every step it discards half of the candidate values of τ still being considered.

This optimization scheme was only tested for both GLSE and SLSE estimation techniques and was used to find the τ with a minimum LSE. Assuming $T = [\tau_1, \tau_2,\ldots,\tau_m]$ to be an array of sorted τ values with $\tau_i < \tau_{i+1}$, bisection method optimization is implemented with the following algorithm:

1. Set $p = floor(length(T)/2)$
2. If $LSE\ (f\ (t, \eta, \tau_p)\ ) > LSE\ (f\ (t, \eta, \tau_{p+1})\ )$, discard from T all elements τ_i such that $i \leq p$, otherwise discard from T all elements τ_i such that $i > p$
3. Repeat steps 1 and 2 until there is only one element in T.
4. Output the remaining element in T as the best time constant estimate.

This algorithm makes use of the fact that the function $LSE\ (f\ (t, \eta, \tau)\ )$ with respect to τ has only one local minima and that its first derivative with respect to τ is always increasing. In a classical sense, the bisection method is a root finding algorithm, however, it has been adapted for the use of curve-fitting to find the root of the derivative with respect to τ of the function $LSE(f\ (t, \eta, \tau_p)\ )$. The only gain that the bisection method has over linear search optimization is that its runtime is much faster. While linear search optimization takes $O(m)$ turns to return a time constant value, the bisection method takes $O(log_2 m)$ turns, which is a significant cut down in runtime.

D. Bisection method shortcomings

Since the bisection method assumes η in exactly the same way that linear search optimization does, it is susceptible to the same failures that linear optimization experiences. There is a significant drop in estimator accuracy and precision for sampled data with a sampling window that is not 'long enough" to assure that the last sampled data point has a strain with a value close to η. The required observation window length is dictated by the value of τ, with longer windows of observation required for time constant curves with higher τ values. Simulations showed that appropriate estimation of η was required for more accurate time constant estimation.

E. Levenberg – Marquardt optimization

The Levenberg-Marquardt (LM) Optimization algorithm is an iterative algorithm based on gradient descent and the Newton method for finding equation roots. The algorithm is especially suited for SLSE minimization (Ranganathan 2004, Levenberg 1944, Marquardt 1963). It is the only optimization algorithm implemented in this study which estimates the best η and τ pair for a given set of noisy temporal strain samples. It was only implemented for the SLSE goodness of fit argument.

As shown earlier, in equation 3.1, LSE curve-fitting involves the minimization of the least square error:

$$LSE(\tau,\eta) = LSE(f(t,\eta,\tau)) = \sum_{i=1}^{n} E(f(t,\eta,\tau), S^{\dagger}(t_i))$$

In the case of SLSE estimation, as shown in equation 3.2 each error metric *E* is defined as:

$$E\left(f(t,\eta,\tau), S^{\dagger}(t_i)\right) = \left(f(t) - S^{\dagger}(t_i)\right)^2$$

As the point of LSE estimation is to minimize it, SLSE minimization is equivalent to minimization with respect to:

$$LSE(f(t,\hat{\eta},\hat{\tau})) = \frac{1}{2}\sum_{i=1}^{n} r_i^2(\hat{\tau},\hat{\eta})$$

where:

$$r_i(\hat{\tau},\hat{\eta}) = S^{\dagger}(t_i) - (\hat{\eta} + (\alpha - \hat{\eta})e^{-\frac{t_i}{\tau}}$$

The parameters τ and η can be vectorized into $x = [\tau, \eta]^T$, where T denotes vector or matrix transpose. Also, allowing $E(x_k) = LSE(f(t,\tau,\eta))$, then, LM optimization follows an update rule of the form:

$$x_{k+1} = x_k - \left(H + \lambda diag\left(diag(H)\right)\right)^{-1} \nabla E(x_k)$$

where $x_k = [\tau_k,\eta_k]$ is the best guess at turn *k*, *H* is the Hessian of *LSE(f,t,x)*, *diag(diag(H))* denotes a diagonal matrix whose non-zero elements are the diagonal elements of matrix *H*. $\nabla E(x_k)$ is the gradient of $E(x_k)$ and λ is a constantly changing step size. λ is picked at each step in the following manner:

1. Evaluate x_{k+1}.
2. If $LSE(f,t,x_{k+1}) > LSE(f,t,x)$

   reject x_{k+1}, retract to x_k and increase λ by a factor of 10

   otherwise, accept x_{k+1} and decrease λ by a factor of 10

In truth, it is possible to increase or decrease λ by factors other than 10. This factor affects the rate of convergence of the algorithm and was set at 10 because this was the factor suggested by the literature (Ranganathan 2004).

F. Challenges with Levenberg-Marquardt optimization

The update rule for finding x_{k+1} shows a few of the issues present in Levenberg-Marquardt optimization. The update involves the calculation of a Hessian matrix, a gradient vector and an inverse matrix. These can all be time-consuming calculations for multiple parameter mathematical models.

Calculation of inverse matrices is notorious for being a time consuming task. However, since this model is dictated mostly by just two parameters, the Hessian matrix *H* is only [2x2]. Therefore the matrix to be inverted is also 2x2. If its determinant is nonzero, then it has an inverse and an explicit formula for the inverse matrix is already well known.

The Hessian matrix:

$$H = \begin{bmatrix} \frac{\delta^2 E(x_k)}{d\tau^2} & \frac{\delta^2 E(x_k)}{d\eta \delta\tau} \\ \frac{\delta^2 E(x_k)}{d\tau \delta\eta} & \frac{\delta^2 E(x_k)}{d\eta^2} \end{bmatrix}$$

involves a lengthy calculation. However, using a quadratic approximation on *E*, *H* can be approximated to $H = J^T J$ where *J* is the Jacobian matrix, whose *i*th row is:

$$J_i = \left[\frac{dr_i(x_k)}{d\tau}, \frac{dr_i(x_k)}{d\eta}\right]$$

The gradient vector:

$$\nabla E(x_k) = \begin{bmatrix} \frac{\delta E(x_k)}{\delta\tau} \\ \frac{\delta E(x_k)}{\delta\eta} \end{bmatrix}$$

can be calculated as:

$$\frac{\delta E(x_k)}{\delta\tau} = \sum_{i=1}^{n} r_i \frac{\delta r_1(x_k)}{\delta\tau}$$

$$\frac{\delta E(x_k)}{\delta\eta} = \sum_{i=1}^{n} r_i \frac{\delta r_1(x_k)}{\delta\eta}$$

Since r_i is already defined for this model, then

$$\frac{\delta r_i(x_k)}{\delta \tau} = -(\alpha - \eta)(\frac{t_i}{\tau^2})e^{-\frac{t_i}{\tau}}$$

$$\frac{\delta E(x_k)}{\delta \eta} = e^{-\frac{t_i}{\tau}} - 1$$

After implementation, the LM optimization scheme along with the SLSE curve-fitting argument were tested with simulations for accuracy, precision, sensitivity and runtime.

CHAPTER V

SIMULATION METHODS AND RESULTS

A. Introduction

All the estimators considered in this study were tested for accuracy, precision, sensitivity, and runtime. These tests were done by simulating sampled noisy time constant curves and using the simulated data as an input for the estimators. Though several algorithms were tested, only the SLSE argument with LM optimization is reported since it is theoretically the most relevant estimators discussed in this study.

B. Simulations

We performed a 1D simulation study to assess accuracy, precision, sensitivity and run-time error of the LM algorithm as a function of the true axial strain time-constant and equilibrium values. Due to the importance of the noise model on the estimation process, selected simulations were repeated for different values of the noise SNR. All simulations were performed in MATLAB and using a desktop computer (Intel Core 2 Duo E4500 @ 2.20 GHz, RAM of 2 GB). The LM results were benchmarked against bisection search results.

The 1D simulations were performed by creating a series of temporal axial strain curves following Eq. (2) with known theoretical τ and η parameters. The maximum

axial strain sampling frequency was fixed at 2 Hz. Such sampling frequency is usually possible in practical elastography systems, which achieve typical frame rates of several frames/sec. It should be noted that low sampling adversely affects the estimators' performance, especially in the case of lower τ values. This implies that the sampling rate needs to be adjusted according to the true τ value as expected from the Nyquist sampling theorem. Figure 1 shows an example of a simulation trial using noisy samples and a corresponding estimated curve obtained using the LM estimator. The dashed line shows the true time constant curve with $\tau = 150\ s$ and $\eta = 0.1$. The dots show the noisy samples $s(t_i)$ input into the LM algorithm and the solid line shows the estimated time constant curve.

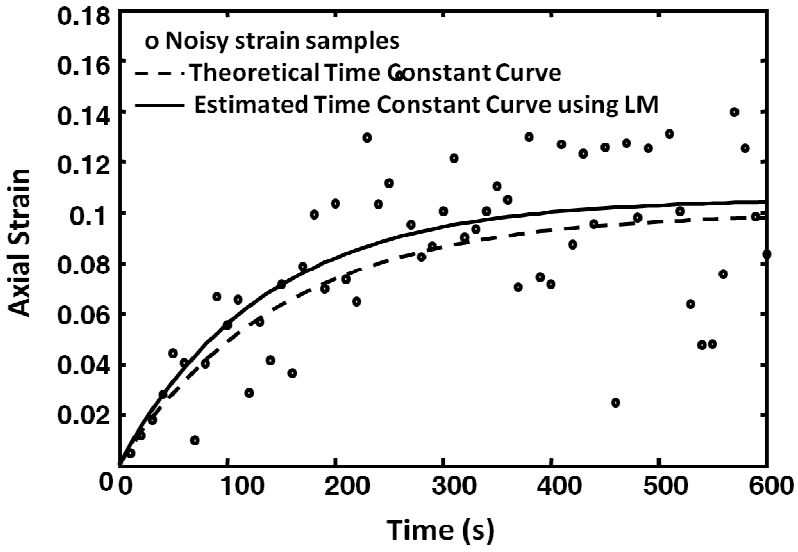

Figure 1 Example of a simulation trial

C. Evaluation of accuracy, precision and runtime

Accuracy and precision were measured in terms of percent deviation and percent spread, respectively. For a given set of *n* trial estimates $\hat{\tau}_i, 1 \leq i \leq n$ done on a set of noisy samples from a time constant curve of known τ, the bias is quantified as the difference between the mean of the measurements and the reference value (in percentage) and the spread is quantified as the standard deviation of the measurements (in percentage), i.e.,:

$$Bias\ (\%) = \left(\frac{|mean\ (\hat{\tau}_i) - \tau|}{\tau}\right) \cdot 100$$

$$Spread\ (\%) = \left(\frac{std\ (\hat{\tau}_i)}{\tau}\right) \cdot 100$$

where *std* denotes the standard deviation. Runtime is calculated as the average processing time it takes to complete each trial.

Accuracy, precision, and runtime were tested for true τ values in the range of 1-800 s and for true η values in the range of 1-20%. We considered two values of window of observations for this study, namely a window of observation of 240 s (i.e., < 0.5 τ_{MAX}) and a window of observation of 600 s (i.e., > 0.5 τ_{MAX}). The choice of these windows of observation allowed practically evaluating the effect of the length of the window of observation (with respect to the true time constant values) on the resulting quality factors. The choice of these windows of observation was dictated by what we believe are practical ranges of window of observations for in vitro and in vivo

elastography applications. For statistical analysis, forty trials were run for each pair of true time constant and equilibrium value.

D. Evaluation of sensitivity

Sensitivity is an important quality factor for the elastographic time constant estimators, which has important implications for the applicability of these estimators in imaging changes in tissue's viscoelastic and poroelastic properties. The sensitivity of the estimator with respect to τ had the goal of determining which would be the smallest increment δ, such that the series of estimates $\hat{\tau}_i$ and $(\widehat{\tau+\delta})_i$ would have statistically different means (at a 95% confidence interval). Due to practical noise considerations and according to some of our preliminary experiments, the smallest increment of δ considered was 1 s. We did not evaluate the estimator's sensitivity with respect to η because we believe that its sensitivity should be very similar to that of the elastography algorithm itself.

E. Evaluation of output signal-to-noise ratio (SNR)

The SNR of the estimators with respect to τ was evaluated using the following equation $SNR = 20\ loglog_{10}\left(\frac{mean\ (\widehat{\tau_i})}{std\ (\widehat{\tau_i})}\right)$. The SNR of the estimators with respect to η was evaluated in a similar manner but considering η in the above equation rather

than τ. The SNR of the estimator was evaluated for two values of input noise SNR (20 dB and 50 dB).

F. Accuracy, precision and runtime results

Figure 2 shows the simulation results of the accuracy study for the LM estimator with respect to τ (figures 2a-b) and η (figures 2c-d) for a window of observation of 240 s (figures 2a-c) and a window of observation of 600 s (figures 2b-d). According to this analysis, the bias in the estimation of both τ and η appears to be close to 1% except for very large values of τ and values of η close to zero. In this difficult scenario, the strain estimates are all similar to each other and almost equal zero. Thus, estimation of the time constant becomes inaccurate regardless of the value of the window of observation used. For the 240 s window of observation, the accuracy appears to start deteriorating for time constants of about 500 s, suggesting that to maintain a bias< 1% the use of a window of observation at least half the time constant is suggested. Note, however, that except for the special case described above, the accuracy of the LM in the estimation of τ is in general below 2% for both values of window of observation. In general, a similar analysis is applicable also to the accuracy of the LM in the estimation of η. Statistical comparison between the results obtained using the two values of window of observation indicates that there is no significant difference (at a 95% confidence level) between the two sets of accuracy results (both for τ and for η) for the range of values of time constant considered.

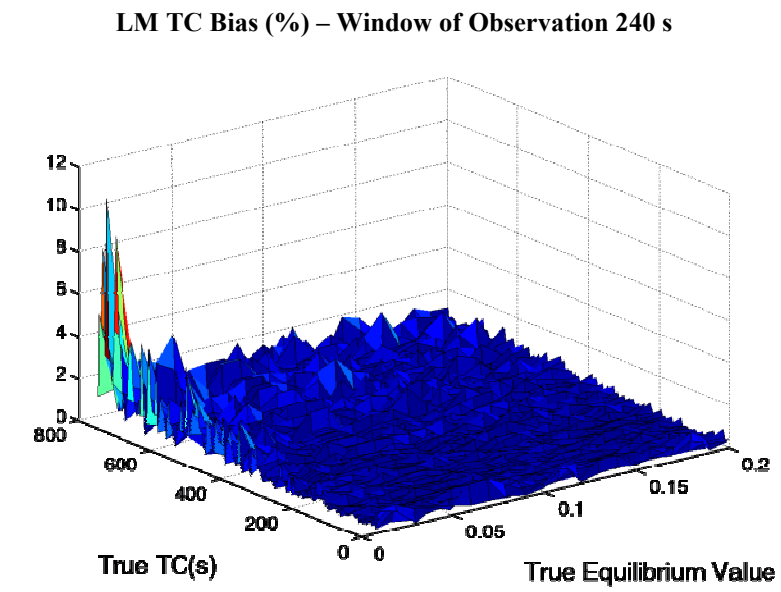

(a)

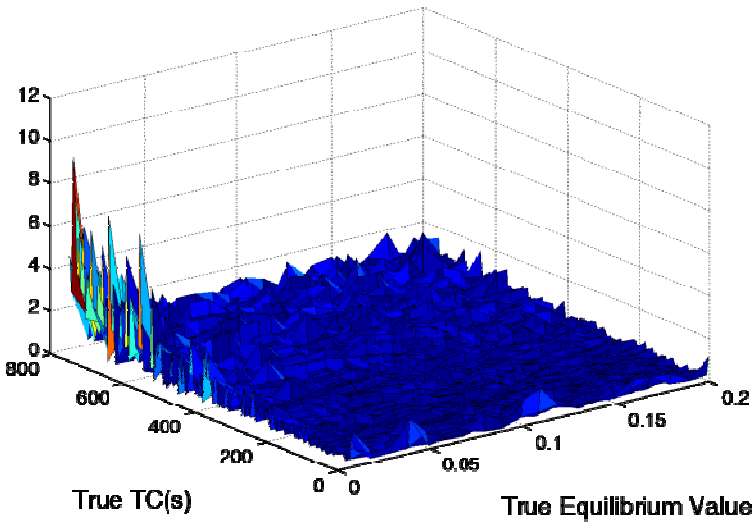

(b)

Figure 2 Percent bias of the LM estimator

LM Equilibrium Point Bias (%) – Window of Observation 240 s

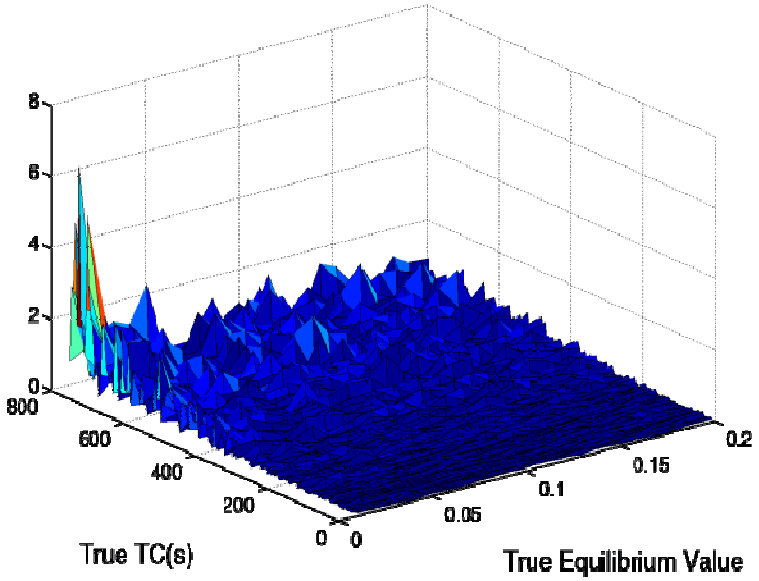

(c)

LM Equilibrium Point Bias (%) – Window of Observation 600 s

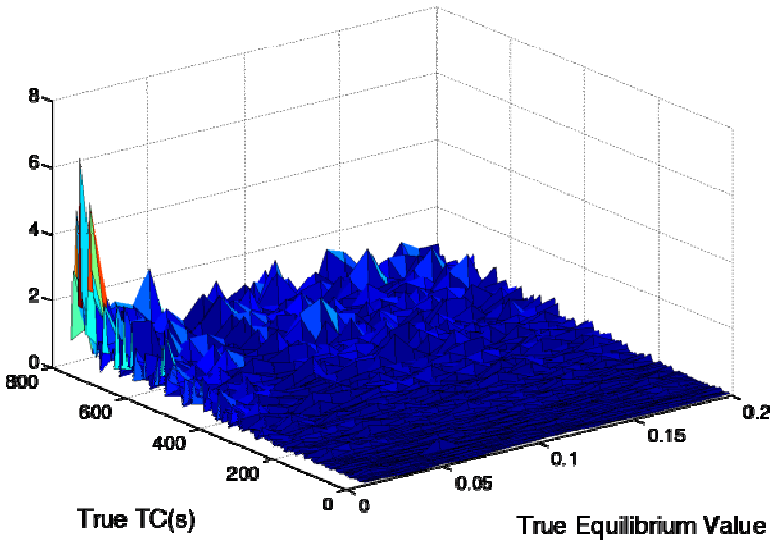

(d)

Figure 2 continued

Figure 3 shows the simulation results of the precision study for the LM estimator with respect to τ (figures 3a-b) and η (figures 3c-d) for a window of observation of 240 s (figures 3a-c) and a window of observation of 600 s (figures 3b-d). As for the accuracy case, we observe low precision for very large values of τ and low values of η. We also observe a deterioration of the precision for very low values of τ, presumably due to insufficient sampling. Overall, the results obtained for the higher window of observation are more precise than those obtained for the lower window of observation (although not statistically significant at a 95% confidence level). This is an expected result because as the window of observation increases, we gain more knowledge about the signal. In general, a similar analysis is applicable also to the precision of the LM in the estimation of η.

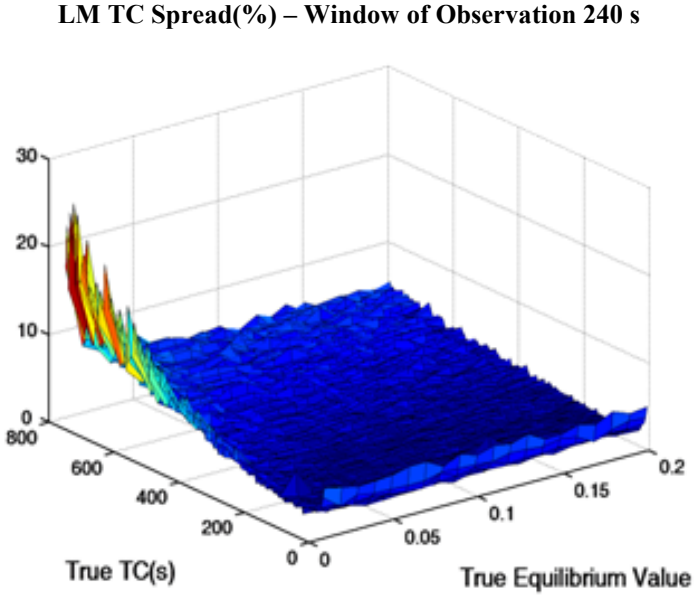

(a)

Figure 3 Percent spread of the LM estimator

LM TC Spread (%) – Window of Observation 600 s

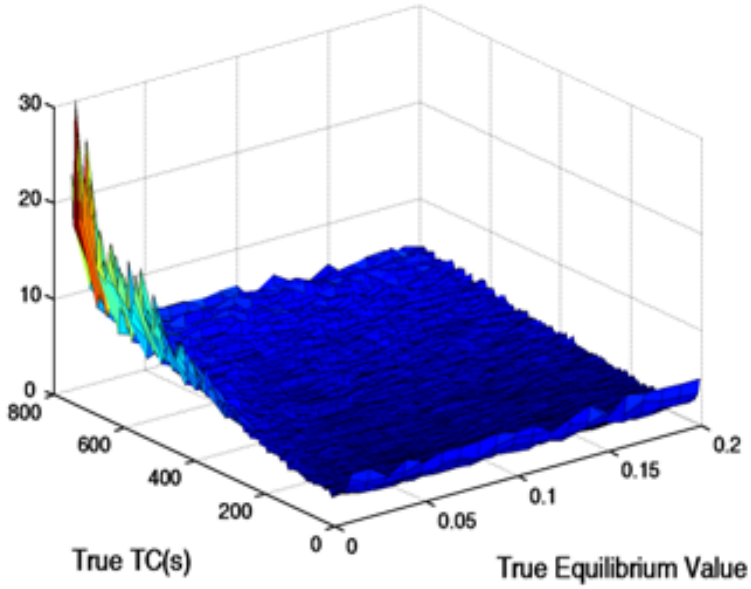

(b)

LM Equilibrium Point Spread (%) – Window of Observation 240 s

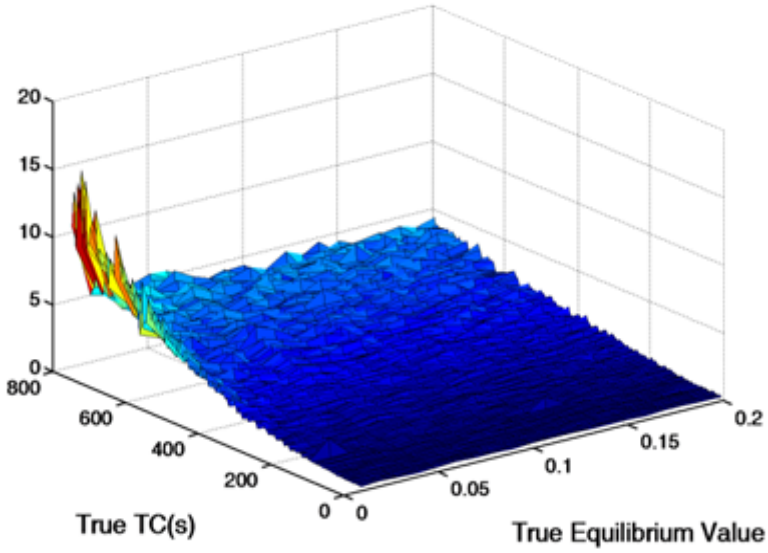

(c)

Figure 3 continued

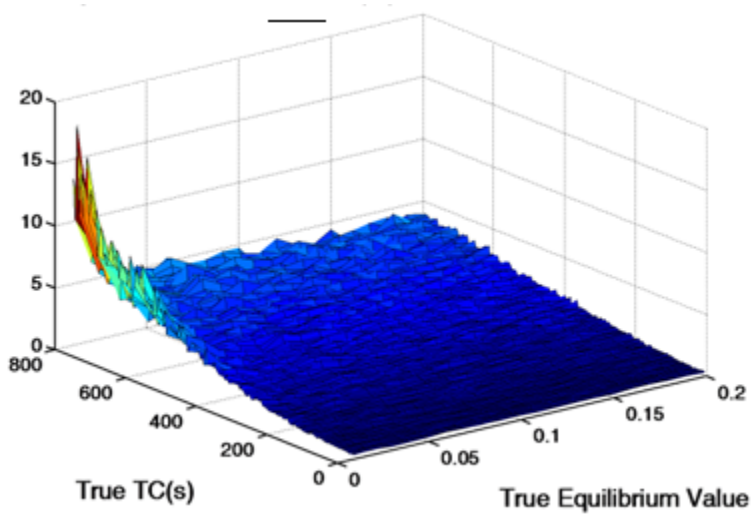

(d)

Figure 3 continued

Figure 4 shows the simulation results of the runtime study for the LM estimator for a window of observation of 240 s (figure 4a) and a window of observation of 600 s (figures 4b). The average processing time per pixel is independent of the size of the window of observation (at a 95% confidence level). As expected, the average time per pixel is also independent with respect to the η value, while it shows an increasing trend with respect to the τ value (although not statistically significant at a 95% confidence level). Based on this simulation study, the LM algorithm can perform fast estimates of $\tau \ and \ \eta$ while maintaining high accuracy and precision.

LM Average Processing Time/Pixel – Window of Observation 240 s

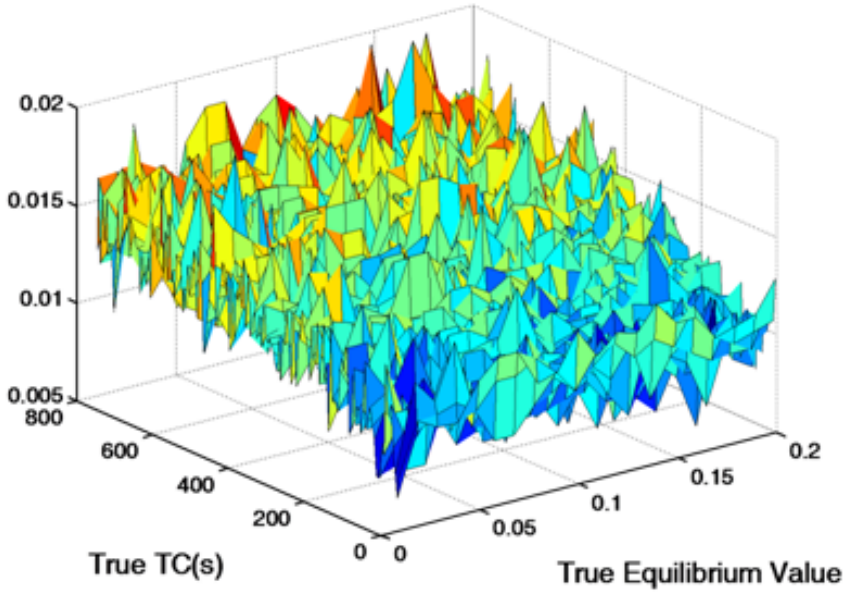

(a)

LM Average Processing Time/Pixel – Window of Observation 600 s

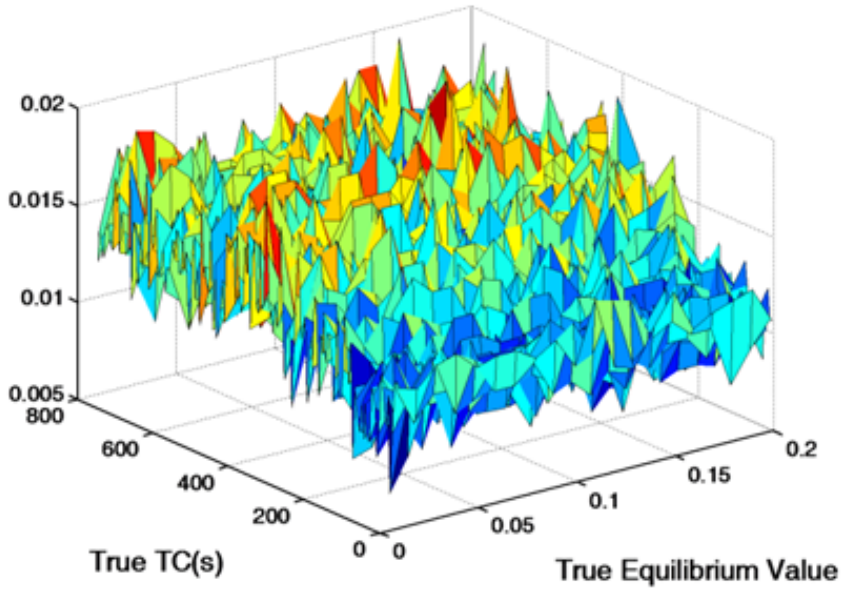

(b)

Figure 4 Average runtime in seconds of the LM estimator

G. Sensitivity

Figure 5 shows the simulation results of the sensitivity study for τ. With respect to sensitivity, this simulation results show a sensitivity (absolute) that depends on the true τ and appears to deteriorate as τ increases. However, if percent sensitivity is considered (i.e., sensitivity over to true time constant), the percent sensitivity of the LM algorithm for τ is at most 1% and actually improves at higher time constants.

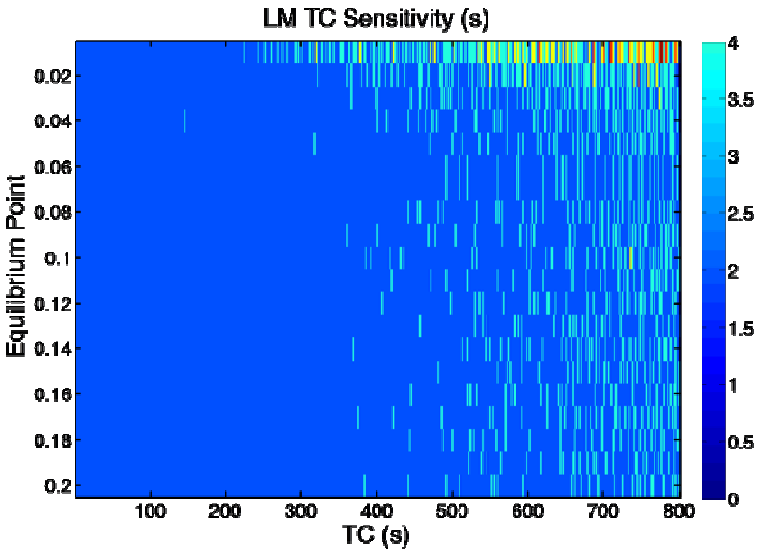

Figure 5 Sensitivity map of the LM estimator for TC estimation

H. Output SNR

Figure 6 shows the simulation results of the SNR study for τ (figures 6a and c) and η (figures 6b and d) and for two values of input noise SNR, 20dB (figures 6a and b)

and 50 dB (figures 6c and d). The results shown in figure 6 correspond to a window of observation of 600 s. Since we observed no statistically significant difference between the results obtained at 240 s and the results obtained at 600 s, the results corresponding to 240 s are not shown.

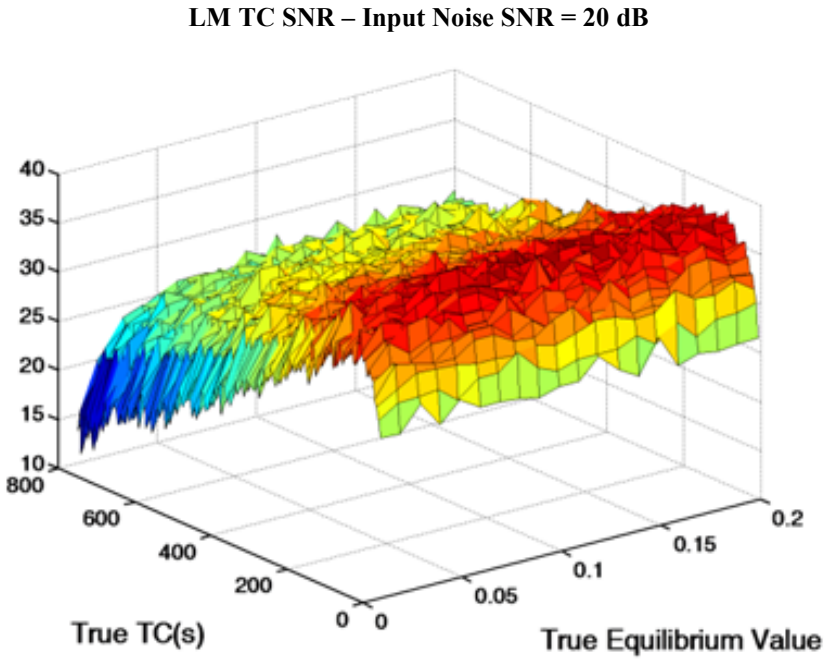

(a)

Figure 6 Output SNR of the LM estimator

LM TC SNR – Input Noise SNR = 50 dB

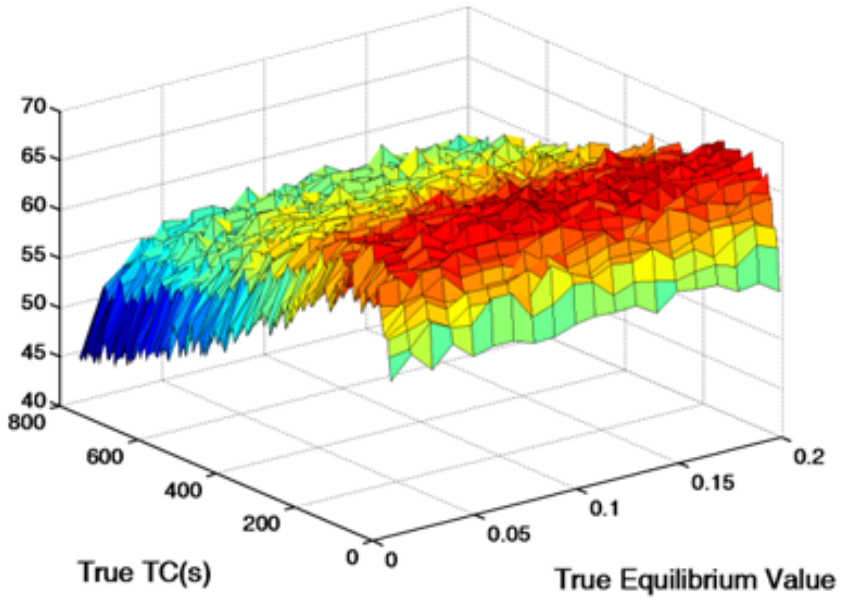

(b)

LM Equilibrium Point SNR – Input Noise SNR = 20 dB

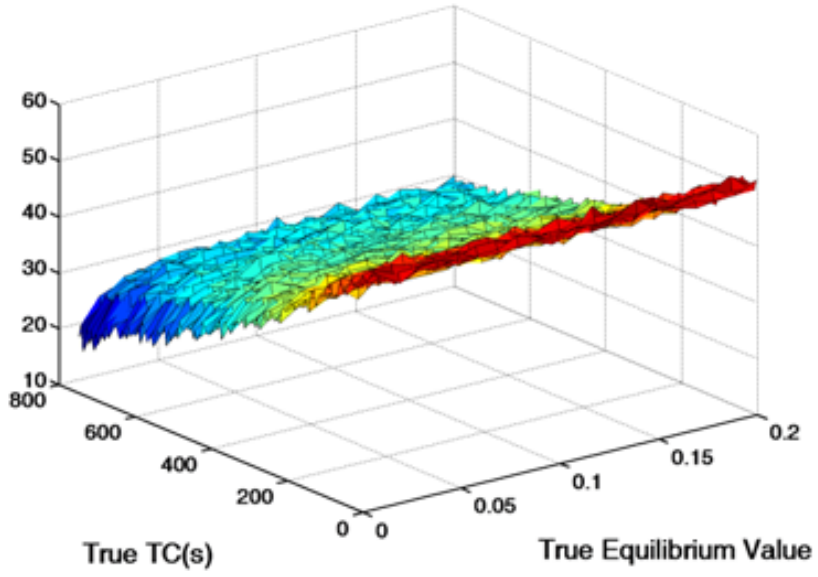

(c)

Figure 6 continued

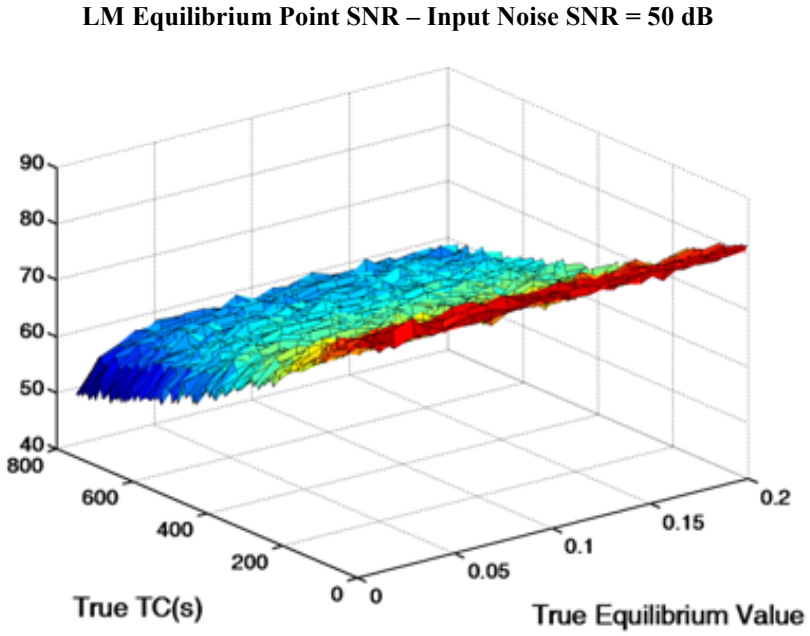

(d)

Figure 6 Continued

In all cases, we observed that the output SNR is affected by the true value of τ but does not depend on the true η. With respect to τ (figures 6a and b), the output SNR for τ remains close to the input noise SNR. i.e., the output SNR is not statistically significantly different than the input SNR (at a 95% confidence level), according to these simulation results being consistently within ± 5 dB with respect to the input SNR. Interestingly, the situation is different in the case of the output SNR for η. This, in fact, is found to be at least equal to and, in many cases, statistically significantly higher than the input noise SNR. These output SNR results can be intuitively explained by the fact that, technically, the LSE curve-fitting estimation behaves as a filter on the strain samples. Thus, as long as the window of observation and the sampling frequency are

sufficiently high, it is possible to produce estimates of τ and η with at least the same input SNR and possibly higher SNR values.

CHAPTER VI

EXPERIMENTAL CORROBORATION

A. Introduction

This chapter discusses the experimental setup and data collection scheme used for this study. These experiments are used just as a proof of principle of the applicability of the axial strain TC estimator to real data.

B. Equipment

Creep tests involve compressing a material under constant force while recording the strain experienced by the material at different points of time. The tissue phantoms used for the experiments were all 4 cm. thick blocks of tofu. Tofu has been shown to mimic the sound properties of tissue very well and is a particularly suitable tissue simulator for ultrasound elastography experiments (Righetti et al. 2004, Righetti et al. 2005, Berry et al. 2006, Wu 2001). The following equipment was used:

- Ultrasonix ultrasound machine
- Custom built compressor to apply creep compression
- Compressor plate
- Water tub

The ultrasound machine is used to collect ultrasound RF data which will be used to create elastograms from which strain vs. time (i.e. creep plots) will be calculated. The exact transducer used is a 38 mm real-time linear array scanner Sonix RP (Ultrasonix, Richmond, BC, Canada) that has 128 elements, a bandwidth between 5-14 MHz, a center frequency of 6.6 MHz, 50% fractional bandwidth at -6 dB, sampling frequency of 40 MHz, and 1 mm beamwidth at the focus.

The creep compressor was built so that an ultrasound transducer could be attached onto a sliding plate thus enabling the transducer to exert a constant force on a material while collecting data from it. The compressor plate is then attached to the transducer as a means to distribute evenly the force around the contact surface area of the tofu block. The use of a tank filled with water was necessary to couple the transducer to the tofu block.

C. Experimental setup

Figure 7 shows a schematic of the experimental setup used to conduct the experiments relevant to this thesis. The schematic shows that the tofu block was submerged in a container filled with water. The sliding plate is part of the custom built compression system that is coupled to two guide rails with ball bearings. The combination of the weights of the transducer, compressor plate and sliding plate is what exerts a constant force on the tofu block.

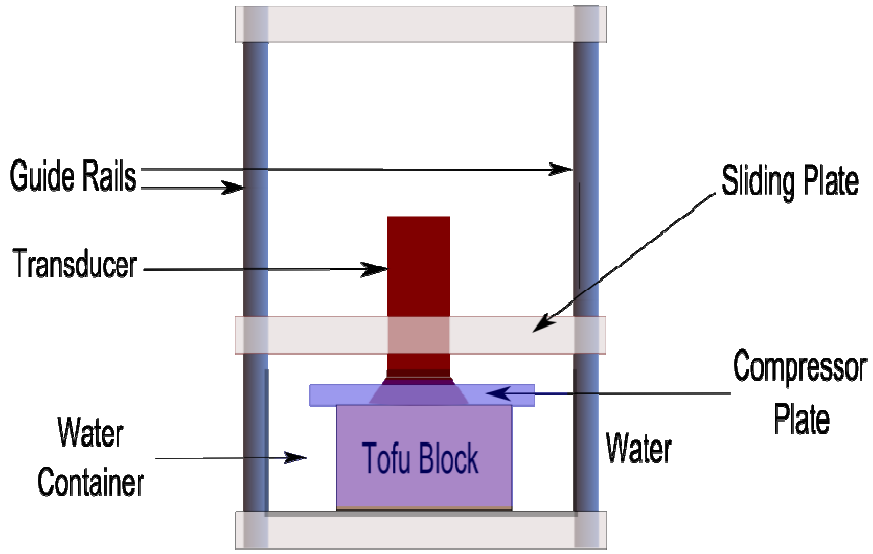

Figure 7 Experimental setup

D. Data collection scheme

The acquisition of a strain vs. time plot involves the collection of ultrasound RF frames at specific intervals of time. The simulations discussed earlier showed that time constant estimation worked better when the strain vs. time plots were sampled at high frequencies. With this in mind, the data collection scheme was set to collect batches of RF frames every 2 seconds for a period of 595 seconds with each batch consisting of 2 frames collected sequentially.

E. Data processing scheme

Since it is not possible to calculate *S(t)* for a large enough *t* by assigning the frame at 0 seconds as the pre-compressed frame and the frame at time *t* as the post-compressed frame, it is necessary to calculate $S(t_i)$ by iterative additive means. Thus, $S(t_i)$ is calculated as:

$$S(t_i) = S(t_{i-1}) + S(t_{i-1}, t_i)$$

with $S(t_1) = S(0,t_1)$. This allows the elastography algorithm to be run on RF frames that are not so distant from each other with respect to time and minimization of decorrelation on noise (Varghese, T. and Ophir, J., 1997).

F. Experimental results

Figure 12 shows typical axial strain time constant elastograms (figures 12a and c) and axial strain equilibrium value elastograms (figures 12b and d) generated using the LM estimator as applied to strain data obtained from a creep experiment conducted on two different tofu phantoms (single realization, no averaging). The tofu phantoms were characterized by different water content. The results shown in figures 12a and b correspond to data obtained from a phantom fully hydrated. The results shown in figures 12c and d correspond to data obtained from the same phantom after partial dehydration. Consistent results were obtained from all tofu phantoms used for this study. The mean value of the axial strain time constant and the equilibrium point shown in figure 12

match well some of our previous results obtained on similar phantoms (Righetti et al. 2007b). The non-uniformity of the spatial distribution of the estimated parameters is typical of the tofu material and consistent with previous experimental work (Righetti et al. 2005). These results show the technical feasibility of using the LM algorithm to generate time constant and equilibrium point elastograms on real, experimental data.

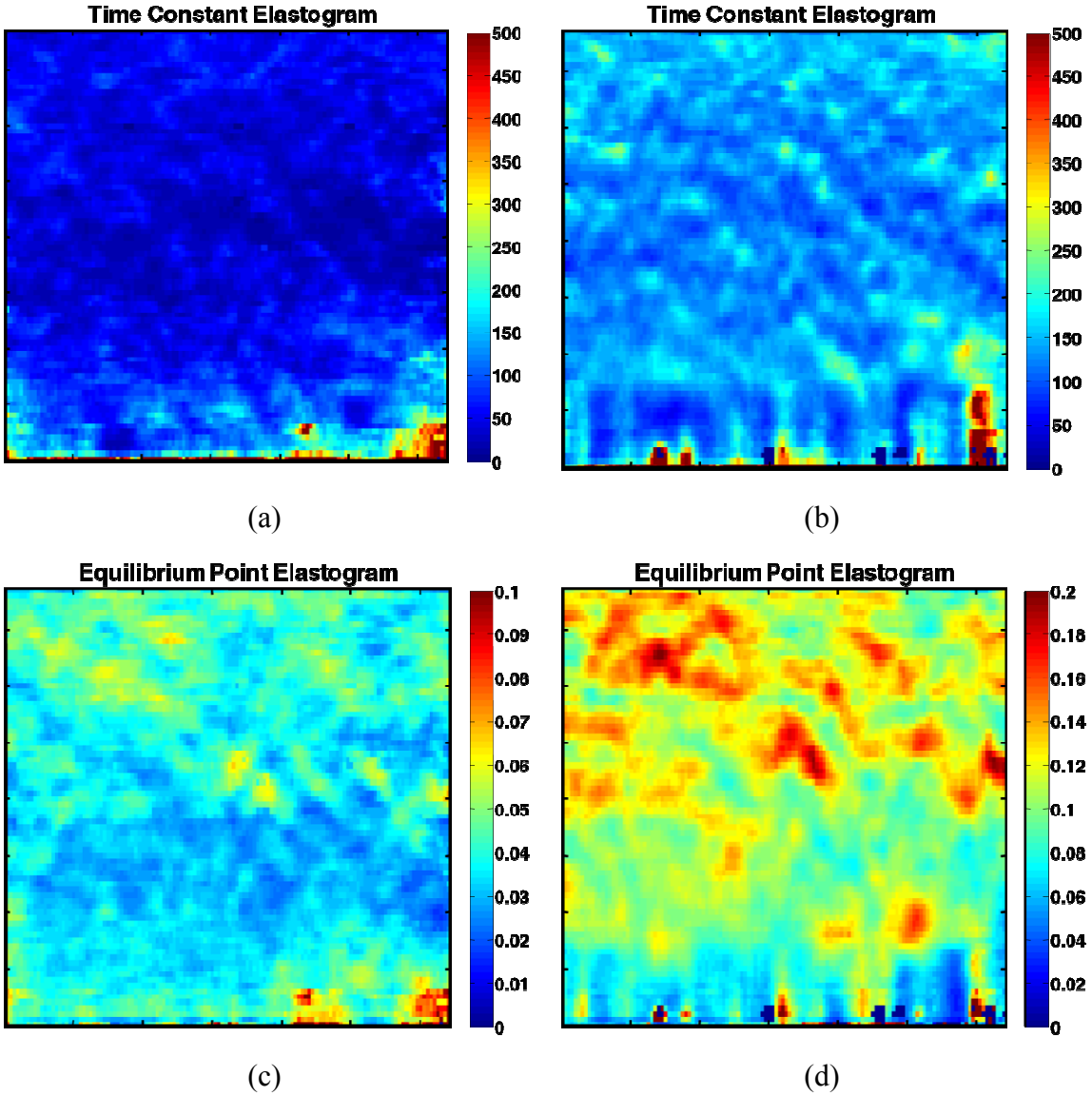

Figure 8 Typical TC and equilibrium point elastograms. Figures were calculated using the LM algorithm. (a) and (c) show results at full hydration and (b) and (d) show results after hydration.

CHAPTER VII

CONCLUSIONS AND FUTURE WORK

A. Introduction

Scientific work is rarely ever concluded as a final product, and is generally to be seen as a step in the correct direction towards progress in knowledge and technology. The study reported in this thesis is by no means an exception to this theory. This chapter discusses a summary of the progress completed in the field by this work and also shares thoughts as to what aspects of this field need further investigation to promote progress.

B. Time constant estimation

The simulated experiments done in this study served the purpose of verifying that the time constant estimator developed for this study was in fact reliable. These experiments revealed that, in a practical sense, the estimators could be trusted to produce accurate and precise results while also being sensitive to changes in τ that were relatively small. This result, though positive, should be used with caution.

As mentioned, while discussing the theory behind standard least square errors curve-fitting (SLSE), the method only returns a probabilistically best estimate whenever each strain is afflicted by Gaussian noise and the distributions of each random variable defining the noise are independent of each other and identically distributed (IID).

However, also mentioned in the study, is the fact that, because of the way each strain value from the strain vs. time plot is calculated, it is impossible to conclude that the noise is in fact IID. Therefore, the SLSE estimators developed in this study return an estimate of the best probabilistically attainable time constant estimate.

This estimate could be improved by implementing a weighted SLSE model where the minimization of the algebraic error for the lower strain values in the strain vs. time plot is given more importance than for the higher values. This is because the standard deviation of the noise of the smaller strain values is smaller than that for higher strain values. Therefore, when considering a candidate time constant curve, a deviation for a small strain value from the candidate curve is less likely to have happened than the same deviation but for a higher strain value.

The biggest challenge with trying to develop a weighted SLSE model is defining the weight assigned to each strain's deviation from a candidate fit. It is natural to conclude that each weight should be a function of the standard deviation of the noise affecting its corresponding strain sample. However, this would require an exact knowledge or an accurate estimate of the standard deviation of the noise distribution affecting each strain. This is in fact a very challenging task, which needs to be studied in future work. Development of accurate noise models of ultrasound strain estimators is an accomplishment that would not only benefit the goal pursued by this study but would also benefit the field of ultrasound elastography in general.

Designing weighted SLSE curve-fitting tools is not the only way with which to improve axial strain time constant imaging. Even if weighted SLSE tools were to be

fully developed, they still would not address the issue that the noise distributions at each strain sample are not independent of each other.

Knowledge of Bayesian theory reveals that when two random variables are independent of each other the situation is in fact undesirable. This is because knowledge of one random variable does not increase knowledge of the other. In this study, the random variable of the noise of a particular strain sample adds a bias to the noise of the next strain sample. The effect of this bias could be reduced by using Bayesian estimators. However, as with the challenge involved in creating weighted SLSE tools, accomplishment of this task is heavily dependent on the development of suitable noise models of the strain estimator itself. This further accentuates the need of an extensive study of the noise affecting each strain estimate.

C. Using GPGPUs for faster processing

The use of General Purpose Graphics Processing Units (GPGPUs), could accelerate the calculation of a time constant image to achieve real-time figures. Yang et al. (2009) have used GPGPUs to successfully generate axial strain elastograms and effective Poisson's ratio elastograms in much less time than traditional CPU-run cross-correlation algorithms and with no loss in elastographic image quality. The reason why GPGPUs are so applicable to axial strain time constant imaging is because it plays to their forte: parallel processing. The creation of TC image involves running the LM algorithm once for each pixel. With GPGPUs it is possible to run this algorithm on

several pixels at once. As well there are several operations inside the LM algorithm, like matrix multiplications, that are also parallelizable. Thus, acceleration using graphics cards could easily turn time-constant imaging into a real-time clinical tool.

D. Confidence metrics

Estimation tools, especially when applied for diagnostic purposes, should be used alongside a measurement of confidence in the estimation. In our group it's common for us to see a correlation map alongside a strain image in order to assess the quality and accuracy of the image. Frequently, for curve-fitting the correlation, R^2, between the determined best fit and the noisy data points is used as a measure of reliability. While it is true that R^2 does give a measure of how 'close' the data points are to the fitted curve and it does actually give some notion of reliability, it suffers from a few downfalls. Firstly, R^2 provides a very non-linear measure of reliability. While this problem could be tackled by correct training of the user or practitioner, the R^2 metric also suffers from not taking into account the number or location of data points used for the estimation/fitting. As an exaggerated example, estimates derived out of three data points can have an R^2 very close to 1, but since only three data points are used, the estimate should not be relied upon for any diagnostic decisions.

The better measure of reliability involves the use of confidence intervals to find a confidence level. The confidence interval (CI) is defined as (Bendat and Piersol 1986):

$$CI = (best\ fit\ parameter + t^{*}error, best\ fit\ parameter - t^{*}error)$$

where t^* is the critical value of a the t-distribution at a particular confidence level for a given degree of freedom. The term "error" refers to a value related to the *LSE* of the best estimate and the shape of the time constant curve. The degree of freedom is defined as the number of data points minus the number of parameters being estimated. The confidence level is a percent value between 0 and 1 that defines the percent certainty with which it can be assured that the actual parameter value lies within the confidence interval. Therefore if the confidence interval is set to a range of acceptability, for example, ±5% of the best fit parameter, then it should be possible to find the confidence level using an inverse t-distribution lookup table. This confidence interval can then be used as a more intuitive measure of reliability.

E. Creep versus stress relaxation

As of now there is some uncertainty as to how exactly experiments should be conducted for measuring time-dependent tissue mechanical parameters. In their study of breast cancer characterization using time-constant imaging, Qiu et al. (2008) created time constant images out of stress-relaxation (constant strain) tests. However, in our study we have been leaning towards the use of creep (constant force) tests. To my knowledge there is no conclusive study that asserts which one is more correct and convenient to use but I think it is necessary to reach a decision about this issue.

F. Clinical applications of TC imaging

It's been mentioned before that time constant imaging could have several applications in lymphedema and cancer imaging. The discrimination between focal benign and malignant tumors by means of ultrasound imaging is an endeavor that has been pursued by several groups (Thomas et al 2006, Thomas et al 2007, Zhi et al 2007, Itoh et al 2006, Qiu et al. 2008).

It should be possible to improve benign-malignant discriminability if several features extractable by elasticity imaging, like EPR and permeability are used in conjunction. After conducting a study on several test subjects with both benign and malignant tumors, it would then be a matter of conducting pattern recognition study to see if in fact discriminability can be improved. The benefits of such a study could reduce the need for invasive biopsy procedures and could potentially also replace x-ray mammograms for ultrasound elastography as a screening tool.

Most of the advances that come to my mind are very application oriented. The tool developed in this study could have uses in sports medicine, cancer imaging, lymphedema tracking and the diagnosis of pathologies that have an effect on time dependent mechanical properties. It is up to the scientific community to explore the diagnostic boundaries that this tool may have.

REFERENCES

Ammann JJ, Rivera R, Ophir J. Rheological modeling of the time-dependent behavior of poroelastic materials under creep test experiments. 5th International Conference on the Ultrasonic Measurement of Tissue Elasticity, Snowbird, UT, October 8-11, 2006.

Bendat JS, Piersol AG. Random Data. Analysis and Measurements Procedures. New York: John Wiley and Sons, 1986.

Berry GP, Bamber JC, Armstrong CG, Miller NR, Barbone PE. Towards an acoustic model-based poroelastic imaging method: I. Theoretical foundation. Ultrasound Med Biol 2006;32(4): 547-567.

Berry GP, Bamber JC, Mortimer PS, Bush NL, Miller NR, Barbone PE.The spatio-temporal strain response of oedematous and nonoedematous tissue to sustained compression in vivo. Ultrasound Med Biol 2008;34(4):617-29.

D'hooge J, Konofagou EE, Jamal F, Heimdal A, Barrios L, Bijmens B, Thoen J, Van de Werf F, Sutherland G, Suetens P. Two-dimensional strain rate measurement of the human heart in vivo. IEEE Trans Ultrason Ferroelec Freq. Control 2002;49: 281–286.

Emilianov SY, Lubinski MA, Weitzel WF, Wiggins RC, Skovoroda AR, O'Donnel M. Elasticity imaging for early detection of renal pathology. Ultrasound Med Biol 1995;21:871-83.

Garra BS, Céspedes EI, Ophir J, Spratt RS, Zuubier RA, Magnant CM, Pennanen MF. Elastography of breast lesions: initial clinical results. Radiology 1997;202(1):79-86.

Hall TJ, Zhu Y, Spalding CS. In vivo real-time freehand palpation imaging. Ultrasound Med Biol 2003;29:427-35.

Itoh A, Ueno E, Tohno E, Kamma H, Takahashi H, Shiina T, Yamakawa M, Matsumura T. Breast disease: clinical application of US elastography for diagnosis. Radiology 2006;239(2): 341-50.

Konofagou EE, Harrigan TP, Ophir J, Krouskop TA. Poroelastography: imaging the poroelastic properties of tissues. Ultrasound Med Biol 2001;27:1387-1397.

Krouskop TA, Vinson S, Goode B, Dougherty D. A pulsed Doppler ultrasonic system for making noninvasive measurements of the mechanical properties of soft tissue. J Rehab Res Dev 1987;24: 1-8.

Levenberg K. A Method for the Solution of Certain Non-Linear Problems in Least Squares. The Quarterly of Applied Mathematics 1944;2:164–68.

Liu D, Ebbini ES. Viscoelastic property measurement in thin tissue constructs using ultrasound. IEEE Trans Ultrason Ferroelectr Freq Control 2008;55(2):368-83.

Donald Marquardt. An Algorithm for Least-Squares Estimation of Nonlinear Parameters. SIAM Journal on Applied Mathematics 1963;11:431–41.

Nilsson James W., and Riedel Susan A. Electric Circuits. New Jersey: Pearson Prentice Hall, 2005.

Qiu Y, Sridhar M, Tsou J K, Lindfors K, Insana M. Ultrasonic Viscoelasticity Imaging of Nonpalpable Breast Tumors: Preliminary Results. Acad Radiol 2008;15:1526-1533.

Ranganathan A. The Levenberg-Marquardt Algorithm. 8th June 2004. http://www.scribd.com/doc/10093320/Levenberg-Marquardt-Algorithm

Righetti R, Garra BS, Mobbs LM, Kraemer-Chant CM, Ophir J, Krouskop TA. The feasibility of using poroelastographic techniques for distinguishing between normal and lymphedematous tissues in vivo. Phys Med Biol 2007a;52(21):6525-41.

Righetti R, Ophir J, Krouskop TA. A method for generating permeability elastograms and Poisson's ratio time-constant elastograms. Ultrasound Med Biol 2005;31(6):803-816.

Righetti R, Ophir J, Srinivasan S, Krouskop TA. The feasibility of using elastography for imaging the Poisson's ratio in porous media. Ultrasound Med Biol 2004;30:215-28.

Righetti R, Righetti M, Ophir J, Krouskop TA. The feasibility of estimating and imaging the mechanical behavior of poroelastic materials using axial strain elastography. Phys Med Biol 2007b;52(11):3241-59.

Sack I, Beierbach B, Hamhaber U, Klatt D, Braun J. Non-invasive measurement of brain viscoelasticity using magnetic resonance elastography. NMR Biomed 2008;21(3):265-71.

Sandrin L, Fourquet B, Hasquenoph JM, Yon S, Fournier C, Mal F, Christidis C, Ziol M, Poulet B, Kazemi F, Beaugrand M, Palau R. Transient elastography: A new noninvasive method for assessment of hepatic fibrosis. Ultrasound Med Biol 2003;29(12):1705-1713.

Sarvazyan A. Mechanical Imaging: a new technology for medical diagnostics. Int J Med Inform 1998;49:195-216.

Shannon C E. Communication in the presence of noise. Proc Institute of Radio Engineers 1949;37(1):10-21.

Souchon R, Rouviere O, Gelet A, Detti V, Srinivasan S, Ophir J, Chapelon JY. Visualization of HIFU lesions using elastography of the human prostate in vivo preliminary results. Ultrasound Med Biol 2003;29:1007-15.

Sridhar M, Insana MF. Ultrasonic measurements of breast viscoelasticity. Med Phys 2007;34(12):4757-67.

Sridhar M, Liu J, Insana MF. Viscoelasticity imaging using ultrasound: parameters and error analysis. Physics in Medicine and Biology 2007;52:2425-2443.

Srinivasan S, Krouskop TA, Ophir J. Comparing elastographic strain images with modulus images obtained using nanoindentation: preliminary results using phantoms and tissue samples. Ultrasound Med Biol 2004;30(3):329-343.

Svensson WE, Usupbaeva A, Shousha S, McLaggan S, Al-Kufaishi A, Thiruchelvam PTR, Lewis JSK, Sinnett HD. Ultrasound elasticity imaging is more accurate than grayscale ultrasound for assessing the extent of invasive breast cancers – early results of pathological correlation. Eur. Radiol 2006;16(Suppl 1):214, 2006.

Thomas A, Kümmel S, Fritzche F, Warm M, Ebert B, Hamm B, Fischer T. Real-time sonoelastography performed in addition to B-mode ultrasound and mammography: improved differentiation of breast lesions. Acad Radiol 2006;13:1496-1504.

Thomas A, Warm M, Hoopmann M, Diekmann F, Fischer T. Tissue Doppler and strain imaging for evaluating tissue elasticity of breast lesions. Acad Radiol 2007;14:522-529.

Varghese, T. and Ophir, J.: A theoretical framework for performance characterization of elastography : The Strain Filter. IEEE Trans Ultrason Ferroel Freq Cont 1997;44:164-172

Wu J. Tofu as a tissue-mimicking material. Ultrasound Med Biol 2001;27:1297-1300.

Yang X, Deka S, Righetti R. Elastography on GPGPU for real-time applications. Proceedings of the 8th International Conference on the ultrasonic measurement and imaging of tissue, Vlissingen, Zeeland, The Netherlands, Sept. 14-17 2009.

Zhi H, Ou B, Luo BM, Feng X, Wen YL, Yang HY. Comparison of ultrasound elastography, mammography, and sonography in the diagnosis of solid breast lesions. J Ultrasound Med 2007;26:807-815.

Supplementary sources

Armstrong CG, Lai WM, Mow VC. An analysis of the unconfined compression of articular cartilage. J Biomech Eng 1984;106:165-173.

Cantrell CA. Technical Note: Review of methods for linear least-squares fitting of data and application to atmospheric chemistry problems. Atmos Chem Phys 2008;8:5477–5487.

Cowin SC, Doty SB. Tissue Mechanics. New York: Springer Science, 2007.

Goldberger AS. A Course in Econometrics. Massachussets: Harvard University Press, 1991.

Gonzalez RC, Woods RE. Digital Image Processing. New Jersey: Prentice Hall, 2008.

Hayes WC and Mockros LF. Viscoelastic properties of human articular cartilage. J Appl Physiol 1971;31:562-568.

Krouskop T A, Wheeler T M, Kallel F, Garra B S and Hall T. Elastic moduli of breast and prostate tissues under compression Ultrason Imaging 1998;20:260-741.

Moon T, Stirling W. Mathematical Methods and Algorithms for Signal Processing. New Jersey: Prentice Hall, 2000.

Mridha M and Ödman S. Noninvasive method for assessment of subcutaneous edema. Med Biol. Eng Comp 1986;24:393-8.

Righetti R, Srinivasan S, Thitai Kumar A, Ophir J and Krouskop TA. Assessing image quality in effective Poisson's ratio elastography and poroelastography – Part I. Physics Med Biol 2007c;52: 1303-1320.

Sarron JC, Blondeau C, Guillaume A, Osmont D. Identification of linear viscoelastic constitutive models. J Biomechanics 2000;33:685-693.

Srinivasan S, Ophir J, Alam SK. Elastographic imaging using staggered strain estimates. Ultrasonic Imag 2002;24:229-245.

Srinivasan S, Righetti R, Ophir J. Trade-offs between the axial resolution and the signal-to-noise ratio in elastography. Ultrasound Med Biol 2003;29:847-66.

Terzaghi K, Peck RB. Soil Mechanics in Engineering Practice. New York: John Wiley and Sons, 1966.

VITA

Name:	Sanjay Padmanabhan Nair
Address:	Department of Electrical and Computer Engineering 2365-H WERC 3128 TAMU College Station, Texas, 77843-3128
Email address:	sanjaynair@neo.tamu.edu
Education:	B.S., Electrical Engineering, Texas A&M University M.S., Electrical Engineering, Texas A&M University